Carbon 172 (2021) 106–111

Contents lists available at ScienceDirect

Carbon

journal homepage: www.elsevier.com/locate/carbon

Research Article

Peierls-type metal-insulator transition in carbon nanostructures

Bing Zhang [a], Ting Zhang [a], Jie Pan [a], Tsz Pong Chow [a], Ammar M. Aboalsaud [b], Zhiping Lai [b, *], Ping Sheng [a, **]

[a] Department of Physics, Hong Kong University of Science and Technology, Clear Water Bay, Kowloon, Hong Kong, China
[b] Division of Physical Sciences and Engineering, King Abdullah University of Science and Technology (KAUST), Thuwal, 23955-6900, Saudi Arabia

ARTICLE INFO

Article history:
Received 2 July 2020
Received in revised form
5 October 2020
Accepted 7 October 2020
Available online 10 October 2020

Keywords:
Carbon nanostructure
(3,0) nanotubes
Peierls transition
Zeolite
Chemical vapor deposition
Fermi level quasigap

ABSTRACT

We report the observation of Peierls-type metal-insulator transition in carbon nanostructures formed by chemical vapor deposition inside the pore network of the ZSM-5 zeolite. The Raman spectrum of this nanocarbon@ZSM-5 indicates a clear signature of the radial breathing mode (RBM) for (3,0) carbon nanotubes that can constitute the carbon network segments. Electrical transport measurements on multiple few-micron-sized nanocarbon@ZSM-5 crystals showed metallic temperature dependence of resistance down to 30 K, at which point the resistance exhibited a sharp upturn that is accompanied by the opening of a quasigap at the Fermi level as indicated by the differential resistance measurements. Further Hall measurements have yielded both the sign of the charge carrier and its density. The latter demonstrated excellent consistency with the quasigap data. We employed first-principles calculations to verify that there can indeed be softening of the phonon modes in the (3,0) carbon nanotubes.

1. Introduction

Zeolites are microporous crystalline aluminosilicates that have uniform porous structures. The pore diameters are in the range between 0.3 nm and 1.2 nm. The robust porous skeletal structure of zeolites has been widely used as catalysts, adsorbents, porous supports, and hosts for making nanomaterials [1,2]. In this work we use the calcined ZSM-5, a type of 10 member-ring zeolite with framework code MFI [3–5], as a template for forming carbon nanostrucutres in its pore network by using the chemical vapor deposition (CVD) method [6]. The skeletal structure of ZSM-5 is shown below in Fig. 1(a); it has straight channels along the b-axis and sinusoidal channels along the a-axis. Both channels have an inner diameter of ~5 Å and interconnected with each other with a segment distance ~10 Å. Each ZSM-5 crystal is about 2–3 μm across, as shown in Fig. 1(b). In contrast to previous works in which 4 Å carbon nanotubes [7–9] were formed inside the linear channels of AFI zeolite [6,10,11], here the nanocarbon@ZSM-5 has a three dimensional (3D) structure. Characterization by Raman spectroscopy indicates a clear radial breathing modes (RBM) peak at 805 cm^{-1} that agrees extremely well with that for the (3,0) carbon nanotube with a diameter of 3 Å. Four-probe electrical resistance measurement on a single zeolite crystal showed a metallic temperature dependence down to 30 K, with a sharp reversal below that temperature. Differential resistance measurements below 30 K showed the development of a quasigap at the Fermi level, which is a signature of the Peierls-type metal-insulator (M I) transition [12–14]. This type of M I transition differs from the more common types of M I transitions in carbon materials such as those induced by molecular doping in graphene [15], by redox doping in single-wall carbon nanotubes [16], or as that in iodinated amorphous carbon films [17]. In addition, charge carriers localization can also lead to M I transition, e.g., in highly disordered carbon fibers [18,19]. Recently, a M I transition was observed in amorphous carbon films that displayed a low temperature magnetic-field-induced conduction channel [20].

To our knowledge, the present work represents the first experimental observation of a Peierls-type transition in carbon nanomaterials. To confirm our interpretation, we have carried out Hall measurements on a single ZSM-5 crystal and obtained the variation of charge carrier density as a function of temperature below 30 K. The Fermi level carrier density showed a sharp decrease below 30 K, in excellent agreement with the differential resistance quasigap data. In contrast to the M–I transition in amorphous carbon films [20], here the transition characteristics do not exhibit any

* Corresponding author.
** Corresponding author.
E-mail addresses: zhiping.lai@kaust.edu.sa (Z. Lai), sheng@ust.hk (P. Sheng).

https://doi.org/10.1016/j.carbon.2020.10.037

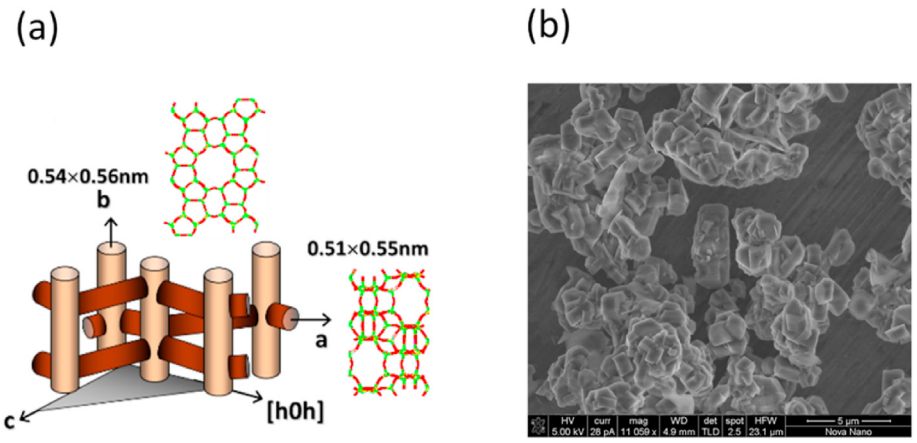

Fig. 1. (a) A cartoon picture of ZSM-5's skeletal pore structure. (b) A SEM image of the ZSM-5's crystals. Each crystal is about 2–3 μm across. (A colour version of this figure can be viewed online.)

magnetic field dependence up to 6 T of applied field.

Theoretical research on Peierls transition was widely studied in one-dimensional carbon materials, such as on single-wall carbon nanotubes CNT(5,5), CNT(3,3), CNT(5,0) [21–25], or in linear carbon chains [26]. In support of our experimental results, we have carried out first-principles calculations on (3,0) nanotubes and showed the existence of phonon soft modes as a result of electron-phonon coupling.

2. Experimental

The nanocarbon@ZSM-5 was grown by using the CVD method. The calcined ZSM-5 zeolite crystals were put in a quartz tube. Five atmosphere pressure of methane (CH_4) was heated to 800 °C for 10 h to grow the carbon nanostructures in the pores of ZSM-5. Subsequent to cooling down, nanocarbon@ZSM-5 was characterized by both Raman spectra and thermal gravimetric analysis (TGA). Results are detailed in the following section.

To measure the transport properties of nanocarbon@ZSM-5, we first deposit a thin layer of photoresist (950 PMMA 9 A) on a quartz substrate. Nanocarbon@ZSM-5 crystals were dispersed on the PMMA and heated on a hotplate at 180 °C for 90 s. This process was helpful to fix the dispersed crystals on the quartz substrate for the subsequent processing. A layer of adhesive Ti with a thickness of 5 nm was coated on the crystals by sputtering, followed by a layer of Au with a thickness of 60 nm. Focused ion beam (FIB) was used to select one crystal, on which the Ti/Au film was etched into a designed square geometric pattern as shown schematically in Fig. 2(a) with the four numbered electrical leads. A scanning electron microscope (SEM) image of the actual device is shown in Fig. 2(b). Due to the small size of the crystals, the traditional six-lead Hall bar geometry was not possible. To measure the longitudinal resistance, current was passed between leads 1 and 2 as shown in Fig. 2(a), and voltage was measured across leads 3 and 4. For the Hall measurements, current was passed between leads 1 and 3 under an applied magnetic field, and voltage was measured across leads 2 and 4.

Measurements of the fabricated device were carried out by using the Physical Property Measurement System (PPMS). A Keithley 6221 was used as the current source and a SR850 lock-in was used as voltmeter to measure the resistance and differential resistance of nanocarbon@ZSM-5.

3. Results and discussion

Measured Raman spectrum is shown in Fig. 3(a). The very high peak at 1604 cm^{-1} is the G band which arises from the vibrations of C–C sp2 bonds. The peak at 1388 cm^{-1} is the D band which arises from the defects in the structure of nanocarbon@ZSM-5. A lower D band peak usually indicates a lower concentration of defects in the sample. We have tried to adjust the fabrication conditions to minimize the defects. The peak at 805 cm^{-1} is the radial breathing modes (RBM) of carbon nanotubes. It is well known that the RBM originates from the coherent vibration of the carbon atoms along the radial direction, which is unique to carbon nanotubes. Normally $\omega_{RBM} = \frac{A}{d} + B$, where $A = 228$, $B = 16$, with d the nanotube diameter in units of nm. Typical RBM range is 100–350 cm^{-1}. From the measured Raman breathing mode data we deduce $d = 0.29$ nm, indicating the nanocarbon@ZSM-5 structure comprises a network of (3,0) carbon nanotubes. From the ab initio calculations as that described in the Supplemental Materials, the RBM frequency of the (3,0) carbon nanotube is around 817 cm^{-1}, very close to the experimentally observed value of 805 cm^{-1}. The RBM of the (2,1) carbon nanotube, 0.236 nm in diameter, is noted to be on the order of 10% higher in frequency. Hence the identification of (3,0) carbon nanotube from its RBM is rather unique. The peak at 1192 cm^{-1} can be due to the combination of RBM and D band modes, usually denoted the intermediate frequency modes (IFM) [8,27,28] that are composed of both first and second-order modes. For comparison, the Raman spectrum for the empty ZSM-5 template is also shown in Fig. 3(a) as the blue curve. It is seen that there are no visible peaks in the relevant frequency range. This comparison indicates that the Raman signal indicated by the black curve in Fig. 3(a) is from the nano-carbon structure.

Results of the TGA measurements on crystals of nanocarbon@ZSM-5 are shown in Fig. 3(b). The sample was placed in the TGA equipment Q5000 and heated in air from room temperature to 800 °C with a heating rate of 2 °C/min. The sample weight was monitored by a microbalance. By burning off the carbon inside the ZSM-5 crystals, we obtained the carbon's weight content from the difference in weight before and during the heating process. As shown in Fig. 2(b) the carbon content of nanocarbon@ZSM-5 is 14.3 wt%. By assuming the carbon structure to be (3,0) carbon nanotubes in each segment of the structure, this TGA result translates into a pore occupation ratio of 35%. Detailed calculation that leads to this number is given in the Supplemental Materials, Section

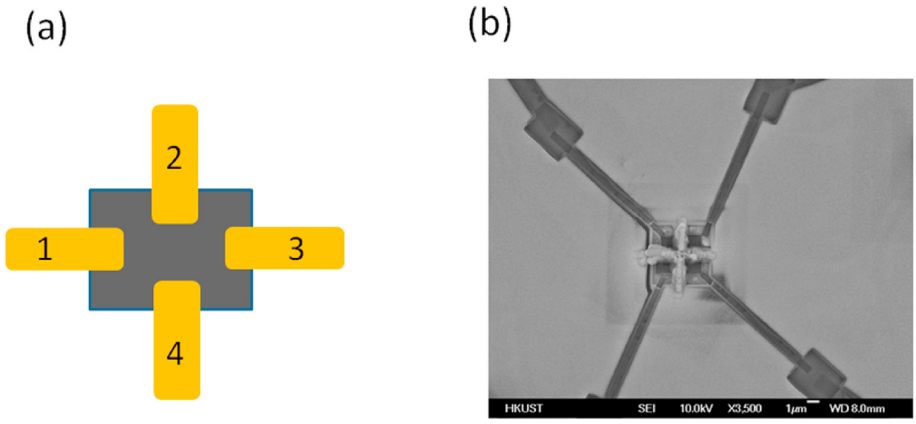

Fig. 2. Device for transport measurement. (a) Schematic illustration of the four-terminal geometry. (b) A SEM image of the four-terminal device for electrical measurement. The size of the nanocarbon@ZSM-5 sample is about 4 μm. (A colour version of this figure can be viewed online.)

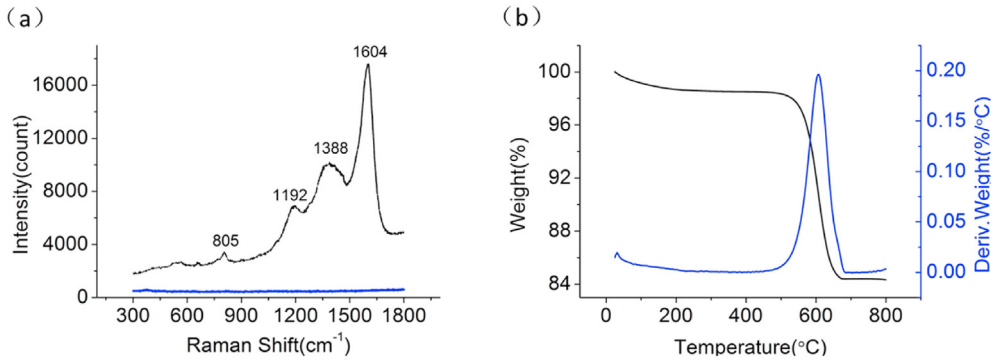

Fig. 3. (a) The Raman spectra of nano-carbon@ZSM-5 (black curve) and empty ZSM-5 template (blue curve), the latter showing no signal, and (b) the thermogravimetric analysis (TGA) of the nano-carbon@ZSM-5 formed by the CVD process. The TGA result shows that the carbon content from the difference in weight before and after the heating process is 14.3 wt%. The blue curve is the differential of the weight loss curve, showing that 600 °C is the decomposition temperature of nanocarbons inside the zeolite pores. (A colour version of this figure can be viewed online.)

A. The derivative of the weight curve (blue) shows a sharp peak at around 600 °C, which indicates the decomposition temperature of nanocarbon structure inside the pores of ZSM-5.

Fig. 4(a) shows the temperature variation of the measured longitudinal resistance in nanocarbon@ZSM-5. Very good linear variation of the resistance, characteristic of metal, is seen from room temperature down to 30 K. However, when the temperature was lowered below 30 K, the resistance is seen to increase quickly. This phenomenon is robust as it appeared in multiple samples. A second sample showing the same metal-insulator transition is shown in the Supplemental Materials, Section B. Differential resistance measurements at four temperatures, plotted as a

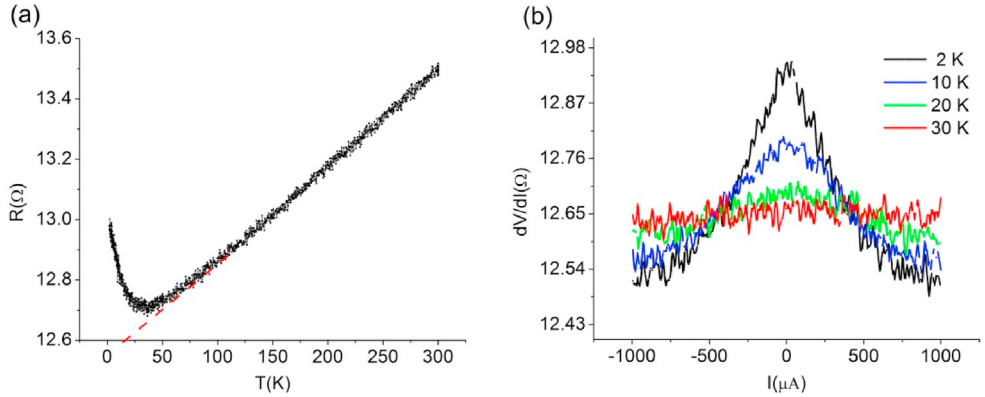

Fig. 4. (a) Measured temperature dependence of resistance for nano-carbon@ZSM-5. A sharp resistance upturn is seen below 30 K. The red dashed line indicates a metallic resistance in series with the Peierls transition component. (b) Measured differential resistance plotted as a function of the driving current. The appearance of a sharp peak at the Fermi level is indicative of the development of a quasigap driven by the soft phonon mode, i.e., a Peierls transition. The sample was measured by the four-terminal configuration shown in Fig. 2(a). (A colour version of this figure can be viewed online.)

function of the driving current, is shown in Fig. 4(b). It shows that the mechanism of the resistance upturn below 30 K is associated with the development of a quasigap centered at the Fermi level. It is seen that at 30 K, the flat differential resistance indicates a linear, Ohmic I–V behavior. However, as the temperature is lowered a clear nonlinear I–V behavior is seen that can be interpreted as the development of a quasigap with an increasing resistance at the Fermi level due to the depletion of charge carriers. The magnitude of the resistance upturn, however, is relatively small, which means that only part of the sample has undergone a Peierls transition. Therefore we should consider the measured resistance to comprise a background resistance that follows the downward linear trend as a function of temperature, shown by the red dashed line in Fig. 4(a), that is in series with the part that has undergone a Peierls transition.

In order to substantiate our interpretation that the upturn in resistance below 30 K is due to the depletion of charge carrier density at the Fermi level, we have carried out Hall measurements under an applied magnetic field. The knowledge of *both the longitudinal and transverse resistance would enable us to separately* determine the mobility and charge carrier density. The results are shown in Fig. 5(a). We know that the Hall resistivity $\rho_{xy} = \frac{B}{ne}$, where B is the magnetic field, n denotes the charge carrier density, and e is the electronic charge. The slope of the Hall resistance is seen to increase with decreasing temperature, indicating a decrease in the charge carrier density at the Fermi level as the temperature is lowered. The data are plotted as black symbols in Fig. 5(b).

Since the longitudinal resistivity is given by $\rho_{xx} = \frac{1}{ne\mu}$, where n denotes the charge carrier density and μ the mobility. If we consider the sample as a Peierls transition component in series with a metallic series resistance (red dashed line in Fig. 4(a)), then we have $\rho_{xx} = \frac{1}{ne\mu} + (aT + b)$, where $aT + b$ is the linear metallic resistance in series as shown by the (extrapolated) red dashed line in Fig. 4(a), with $a = 3.23 \times 10^{-3}\Omega T^{-1}$ and $b = 10.80\Omega$. By fitting the longitudinal resistance data at temperatures higher than 30 K, we obtain the mobility value to be $\mu = 13.06\ cm^2V^{-1}s^{-1}$, which is lower than that in the plane of graphite, $\mu = 9.0 \times 10^4\ cm^2V^{-1}s^{-1}$ [29]. By assuming the mobility value to be a constant over the relevant temperature range, the value of n can be directly obtained from the peak value of the differential resistance data in Fig. 4(b) (as it corresponds to the Fermi level). The charge carrier density obtained in this manner is plotted as red symbols in Fig. 5(b). We can see that the agreement is excellent, which not only confirms our assumption that the mobility is constant over the relevant temperature range, but also leads to the conclusion that a Peierls-type M–I transition has indeed occurred through the opening of a quasigap in the Fermi level charge carrier density.

4. Theoretical considerations

Peierls-type MI transition owes its origin in the electron-phonon coupling and the one-dimensional geometry. Since the ZSM-5 zeolite pores comprise intersecting one-dimensional channels with 5 Å inner diameter, (3,0) CNT can be accommodated. Here we would like to consider the nanocarbon@ZSM-5 to consist of (3,0) CNT segments, which is supported by the Raman RBM signal at 805 cm^{-1}. This value is very close to the ab-initio estimation of the RBM for the (3,0) CNT at 817 cm^{-1}. Our theoretical consideration is to see if the (3,0) CNT can have phonon softening, which is a necessary condition (but may not be sufficient) for the nanocarbon@ZSM-5 to exhibit a Peierls-type M–I transition [12,13].

In a Peierls process the lattice distorts (usually dimerizes) and opens a gap at the Fermi level, thereby makes the system transit from a metal to an insulator at zero temperature. In such a process the equilibrium positions of atoms change, causing an increase in the elastic energy. However, distortion of the atomic lattice simultaneously opens a gap in the electronic band structure at the Fermi level and lowers the electronic energy. As the latter more than compensates the increase in the elastic energy, hence this is an instability that can occur with especially high inevitability in 1D metals. However, if the atomic bonding is strong, the Peierls transition temperature can be low. We have carried out ab-inito calculations on the (3,0) CNTs. The calculational details are given in the Supplemental Materials, Section C. Our estimation shows that the (3,0) CNT can indeed have phonon softening that undergoes a Peierls transition under T_p ~273 K. The relevant soft phonon mode of (3,0) CNT is illustrated in Fig. 6. We have to recognize, though, that the present nanocarbon@ZSM-5 is a 3D network of 1D segments, hence the theory necessarily over-estimate the Peierls transition temperature.

The existence of the Peierls-type transition in nanocarbon@ZSM-5 implies a reasonably large electron-phonon coupling. Since superconductivity is another consequence of electron-phonon coupling, in the earlier theoretical works [30,31] we have found that better screening of Coulomb interaction among the electrons, which is a negative element for superconductivity, can greatly suppress the Peierls transition while simultaneously enhance the superconductivity transition. As a result, our next experimental effort is along the direction of providing better Coulomb screening, with the intention to see if a superconducting ground state can be accomplished in this system.

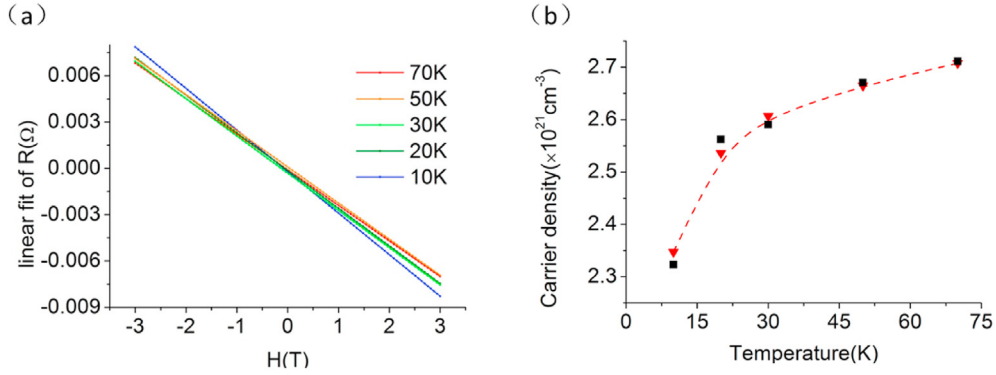

Fig. 5. (a) The temperature dependence of Hall resistance for nano-carbon@ZSM-5. (b) A comparison between the electronic charge carrier density obtained from by the Hall measurements (black symbols) and that obtained from fitting of the longitudinal differential resistance peak values vs. temperature in nano-carbon@ZSM-5 (red symbols). The red dashed curve is to guide the eye. (A colour version of this figure can be viewed online.)

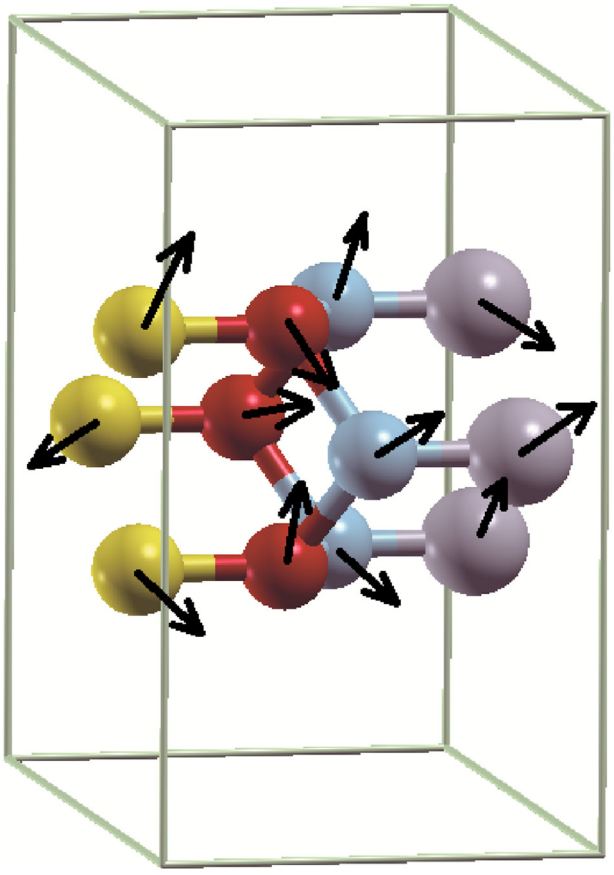

Fig. 6. The unit cell of (3,0) CNT consists of four triangular layers of carbon atoms, with two registered layers in the back rotated 60° with respect to the two registered layers in the front. Here each layer is identified with a different color from the other layers, to facilitate easy visualization. The arrows shown in the figure indicate the magnitude and direction of the displacement for each atom in the soft phonon mode with $q = 0.45/a$, where a is the length of the unit cell. (A colour version of this figure can be viewed online.)

5. Conclusions

By making use of the ZSM-5 zeolite as the template we have successfully fabricated nano-carbon@ZSM-5 with a high pore filling factor (35%) 35 . The Raman spectrum of nanocarbon@ZSM-5 exhibits a RBM peak around 805 cm^{-1}, indicating the nanocarbon@ZSM-5 to comprise segments of the smallest carbon nanotube (3,0). The resistance of the nanocarbon@ZSM-5 displays a metal to insulator transition at 30 K. This interesting phenomenon can be explained by the Peierls-type transition that opens a gap at the Fermi level. By carrying out resistance and Hall measurements we found consistency between the Hall measurement and the differential resistance measurement that clearly indicates the opening of a quasigap at the Fermi level. First-principles calculations on (3,0) CNT were carried out, with the results showing a Peierls transition can indeed occur.

CRediT authorship contribution statement

Bing Zhang: Methodology, Validation, Investigation, Writing - original draft, Writing - review & editing. **Ting Zhang:** Methodology, Software, Writing - review & editing. **Jie Pan:** Investigation. **Tsz Pong Chow:** Investigation. **Ammar M. Aboalsaud:** Resources, Investigation. **Zhiping Lai:** Resources, Supervision, Project administration, Funding acquisition, Writing - review & editing. **Ping Sheng:** Conceptualization, Methodology, Formal analysis, Supervision, Writing - original draft, Writing - review & editing, Funding acquisition.

Declaration of competing interest

The authors declare that they have no known competing financial interests or personal relationships that could have appeared to influence the work reported in this paper.

Acknowledgements

P. S. wishes to acknowledge support by the Research Grants Council of Hong Kong, Grant 16308216, and by collaborative grant from KAUST, Saudi Arabia KAUST18SC01. Z. Lai wishes to acknowledge the KAUST competitive research grant URF/1/3435–01.

Appendix A. Supplementary data

Supplementary data to this article can be found online at https://doi.org/10.1016/j.carbon.2020.10.037.

References

[1] S.M. Auerbach, K.A. Carrado, P.K. Dutta, Handbook of Zeolite Science and Technology, CRC Press, 2003.
[2] K. Kim, T. Lee, Y. Kwon, Y. Seo, J. Song, J.K. Park, H. Lee, J.Y. Park, H. Ihee, S.J. Cho, Lanthanum-catalysed synthesis of microporous 3D graphene-like carbons in a zeolite template, Nature 535 (7610) (2016) 131–135.
[3] G. Kokotailo, S. Lawton, D. Olson, W. Meier, Structure of synthetic zeolite ZSM-5, Nature 272 (5652) (1978) 437–438.
[4] Y. Yan, M.E. Davis, G.R. Gavalas, Preparation of zeolite ZSM-5 membranes by in-situ crystallization on porous. Alpha.-Al2O3, Ind. Eng. Chem. Res. 34 (5) (1995) 1652–1661.
[5] W. Xu, J. Dong, J. Li, J. Li, F. Wu, A novel method for the preparation of zeolite ZSM-5, J. Chem. Soc., Chem. Commun. (10) (1990) 755–756.
[6] B. Zhang, Y. Liu, Q. Chen, Z. Lai, P. Sheng, Observation of high Tc one-dimensional superconductivity in 4 Angstrom carbon nanotube arrays, AIP Adv. 7 (2) (2017), 025305.
[7] S. Iijima, Helical microtubules of graphitic carbon, Nature 354 (6348) (1991) 56–58.
[8] A. Oberlin, M. Endo, T. Koyama, Filamentous growth of carbon through benzene decomposition, J. Cryst. Growth 32 (3) (1976) 335–349.
[9] G. Dresselhaus, S. Riichiro, Physical Properties of Carbon Nanotubes, World Scientific, 1998.
[10] N. Wang, Z.-K. Tang, G.-D. Li, J. Chen, Single-walled 4 Å carbon nanotube arrays, Nature 408 (6808) (2000) 50–51.
[11] Z. Tang, L. Zhang, N. Wang, X. Zhang, G. Wen, G. Li, J. Wang, C.T. Chan, P. Sheng, Superconductivity in 4 angstrom single-walled carbon nanotubes, Science 292 (5526) (2001) 2462–2465.
[12] R.E. Peierls, Quantum Theory of Solids, Clarendon Press, 1996.
[13] R.H. McKenzie, Microscopic theory of the pseudogap and Peierls transition in quasi-one-dimensional materials, Phys. Rev. B 52 (23) (1995) 16428.
[14] P.A. Lee, T. Rice, P. Anderson, Fluctuation effects at a Peierls transition, Phys. Rev. Lett. 31 (7) (1973) 462.
[15] S. Zhou, D. Siegel, A. Fedorov, A. Lanzara, Metal to insulator transition in epitaxial graphene induced by molecular doping, Phys. Rev. Lett. 101 (8) (2008), 086402.
[16] J. Vavro, J. Kikkawa, J.E. Fischer, Metal-insulator transition in doped single-wall carbon nanotubes, Phys. Rev. B 71 (15) (2005) 155410.
[17] L. Kumari, S. Subramanyam, S. Eto, K. Takai, T. Enoki, Metal–insulator transition in iodinated amorphous conducting carbon films, Carbon 42 (11) (2004) 2133–2137.
[18] K. Kuriyama, M. Dresselhaus, Metal-insulator transition in highly disordered carbon fibers, J. Mater. Res. 7 (4) (1992) 940–945.
[19] A. Fung, M. Dresselhaus, M. Endo, Transport properties near the metal-insulator transition in heat-treated activatedrotect carbon fibers, Phys. Rev. B 48 (20) (1993) 14953.
[20] Z. Liu, C. Zhen, P. Wang, C. Wu, L. Ma, D. Hou, Metal-insulator transition and novel magnetoresistance effects in amorphous carbon films, Carbon 148 (2019) 512–517.
[21] A. Sédéki, L. Caron, C. Bourbonnais, Electron-phonon coupling and Peierls transition in metallic carbon nanotubes, Phys. Rev. B 62 (11) (2000) 6975.
[22] K.-P. Bohnen, R. Heid, H. Liu, C. Chan, Lattice dynamics and electron-phonon interaction in (3, 3) carbon nanotubes, Phys. Rev. Lett. 93 (24) (2004) 245501.
[23] D. Connétable, G.-M. Rignanese, J.-C. Charlier, X. Blase, Room temperature Peierls distortion in small diameter nanotubes, Phys. Rev. Lett. 94 (1) (2005), 015503.
[24] M.T. Figge, M. Mostovoy, J. Knoester, Peierls transition with acoustic phonons

and solitwistons in carbon nanotubes, Phys. Rev. Lett. 86 (20) (2001) 4572.
[25] G. Dumont, P. Boulanger, M. Côté, M. Ernzerhof, Peierls instability in carbon nanotubes: a first-principles study, Phys. Rev. B 82 (3) (2010), 035419.
[26] A. Milani, M. Tommasini, D. Fazzi, C. Castiglioni, M.D. Zoppo, G. Zerbi, First-principles calculation of the Peierls distortion in an infinite linear carbon chain: the contribution of Raman spectroscopy, J. Raman Spectrosc. 39 (2) (2008) 164–168.
[27] C. Fantini, A. Jorio, M. Souza, L. Ladeira, A. Souza Filho, R. Saito, G.G. Samsonidze, G. Dresselhaus, M. Dresselhaus, M. Pimenta, One-dimensional character of combination modes in the resonance Raman scattering of carbon nanotubes, Phys. Rev. Lett. 93 (8) (2004), 087401.
[28] C. Fantini, M. Pimenta, M. Strano, Two-phonon combination Raman modes in covalently functionalized single-wall carbon nanotubes, J. Phys. Chem. C 112 (34) (2008) 13150–13155.
[29] D. Soule, Magnetic field dependence of the Hall effect and magnetoresistance in graphite single crystals, Phys. Rev. 112 (3) (1958) 698.
[30] T. Zhang, P. Sheng, Superconducting versus semiconducting electronic ground state in chirality-specific double-wall carbon nanotubes, New J. Phys. 15 (8) (2013), 083021.
[31] T. Zhang, M.Y. Sun, Z. Wang, W. Shi, P. Sheng, Crossover from Peierls distortion to one-dimensional superconductivity in arrays of (5, 0) carbon nanotubes, Phys. Rev. B 84 (24) (2011) 245449.